Int J Adv Manuf Technol (2017) 91:2919–2931
DOI 10.1007/s00170-016-9527-y

ORIGINAL ARTICLE

Effect of process parameters on microstructure and mechanical properties of friction stir-welded Ti–6Al–4V joints

A. Fall[1] · **M. Jahazi**[1] · **A. R. Khdabandeh**[2] · **M. H. Fesharaki**[2]

Received: 21 June 2016 / Accepted: 25 September 2016 / Published online: 10 October 2016

Abstract In this work, the microstructure and mechanical behavior of friction stir-welded 2-mm-thick sheets of Ti–6Al–4V alloy were investigated. Specifically, the influence of friction stir welding (FSW) process parameters on microstructure evolution, defect generation, tensile, and hardness properties of the joint were studied. Optical and scanning electron microscopies were used to examine the microstructure and to determine the type and nature of the defects. A progressive change in the microstructure from equiaxed and elongated α grains (base metal) to a very fine lamellar structure with an average grain size of less than 1 μm (in the upper stir zone) was observed and related to FSW parameters. Tensile tests and microhardness measurements were also carried out to assess the mechanical properties. Important variations were observed on tensile strength and hardness distribution as a function of process parameters. The weakest mechanical properties and fracture were found in the heat-affected zone (HAZ) of the as-welded joints. The results were analyzed in terms of the pseudo heat index, and it was determined that tool rotation is the most significant process parameter influencing both the microstructure and mechanical properties of FSWed Ti–6Al–4V joints.

Keywords Friction stir welding · Tensile test · Microstructure · EBSD · SEM · Microhardness

The original version of this article was revised: This article originally published with the author family name incorrectly listed. The author name have now been appear correctly above.

Submitting highlights Ti–6Al–4V plates with a thickness of 2 mm were successfully friction stir welded under different welding conditions. The mechanical properties of the joint were investigated by using tensile test and microhardness measurements for different welding heat index parameters.
The following conclusions can be drawn from this study:
1. The heterogeneous distributions of mechanical properties were directly related to the microstructure. It was shown that the SZ has the highest mechanical properties while the HAZ is the weakest region in the weld. The mechanical properties of the HAZ can be associated with the transverse tensile properties of the weld.
2. Mechanical properties of the FSW joint were correlated with the change in the microstructure, mainly in grain size distribution. In addition, the $\beta \rightarrow \alpha + \beta$ phase transition in titanium alloys strongly influences microstructure evolution and therefore affects the mechanical properties of the joint.
3. The heat index ratio can be used as a reliable parameter to describe the variations in strength and ductility of the joint.
4. The combined influence of temperature and strain, rather than temperature alone, is the key factor affecting the mechanical properties of the joint. Therefore, the tool rotational speed and the tool travel speed should be properly controlled to ensure good mechanical properties in FSWed Ti–6Al–4V alloys.

✉ A. Fall
ameth-maloum.fall.1@ens.etsmtl.ca

[1] Ecole de Technologie Supérieure (E.T.S.), Département de Génie Mécanique, 1100 Rue Notre-Dame Ouest, Montréal, QC H3C 1K3, Canada

[2] Science and Research Branch, Islamic Azad University, Teheran, Hesarak, Iran

1 Introduction

The trend in design and fabrication of aerospace structures is moving rapidly toward the use of carbon fiber polymer composite materials and the consolidation of many pieces into large monolithic assemblies. Titanium and its alloys because of their higher specific strength, closer match to their coefficient of thermal expansion, and superior corrosion resistance are more compatible with composite materials than aluminum alloys [1, 2]. Therefore, there is a need to produce large size structures made of titanium that would be used to assemble different components made of composite materials. However,

due to the large size of the structures, the titanium parts need to be welded together first.

Ti and Ti alloys are currently welded by almost all conventional fusion welding processes including gas tungsten arc welding (GTAW), gas metal arc welding (GMAW), plasma arc welding (PAW), electron beam welding (EBW), and laser beam welding (LBW) [3, 4]. However, fusion-welded components are rarely used in aircraft structural components due to the formation of brittle coarse microstructure, the presence of high residual stress, and the severe deformation after welding inherent to these techniques.

Friction stir welding (FSW), as a solid-state welding process, is one of the most promising techniques for joining titanium alloys avoiding a large number of the abovementioned difficulties and therefore could be used for the manufacturing of large size components for aerospace applications [5, 6]. Moreover, Ti FSW could be also used as an alternative manufacturing technology in the fabrication process of hollow components traditionally produced by a combination of diffusion bonding and superplastic forming [7, 8].

However, many challenges are still faced in FSW of titanium alloys which are related to the physical and mechanical properties of titanium. The main difficulties arise from a combination of tool materials and geometry for efficient stirring, low thermal conductivity, and the temperature dependence of flow stress [7]. The high strength and elevated temperatures required to friction stir weld titanium, in combination with the chemical reactivity of titanium, limit possible tool materials that can be used to friction stir weld these alloys when compared with aluminum and its alloys. Specifically, while a large variety of tool geometries are used for aluminum alloys, those for FSW of titanium alloys are very simple and do not generate the intense vertical material flow typically observed in aluminum friction stir welds. On the other hand, titanium's moderate thermal conductivity and high heat capacity significantly inhibit heat transfer away from the tool. Thus, heat generated from the shoulder is ineffective for heating the base of the weld, establishing a thermal gradient through the thickness of the weld that only worsens for thicker sections. Furthermore, the large temperature dependence of the flow stress, characteristic of titanium alloys, [9] will generate high gradients in flow stress through the thickness of the material which may prevent maintaining suitable welding conditions resulting in defect generation.

Previous works in FSW of titanium and its alloys have shown significant grain size refinement and increase in hardness in the stir zone (SZ) [6, 10]. However, little data is available on the role of welding parameters, such as the heat generated by the shoulder and the tool rotation, on microstructure and mechanical properties of the Ti FSWed joints.

In the present work, using fixed tool geometry, Ti–6Al–4V sheets were friction stir welded for different tool rotation and tool traverse speeds. The microstructural characteristics of the joints as well as their mechanical properties were analyzed. Moreover, the impact of each process parameter on microhardness and tensile properties was quantified, and the most influential process parameter was identified. The process conditions leading to optimum mechanical properties were determined, and the corresponding microstructure and mechanical properties were documented.

2 Experimental materials and methods

The material used in the present investigation was annealed 2-mm sheets of Ti–6Al–4V alloy with the following chemical composition (wt%): Al 6.09, V 4.02, C 0.011, Fe 0.14, N 0.008, H 0.0023, and balance Ti. The mechanical properties of the as-received material are provided in Table 1.

The as-received sheets were butt-welded as shown in Fig. 1a. For reference, WD corresponds to the welding direction and is parallel to the transverse direction (TD), while ND stands for the normal direction and cross welding (CW) represents the rolling direction. The welding was performed on two plates, 100 mm in length and 50 mm in width by using a stainless steel backing plate and a W carbide-based alloy tool with a 15-mm shoulder diameter, 6-mm probe diameter, and 1.8-mm probe length as shown in Fig. 1b. Argon shielding gas was continuously employed to prevent oxidation of the joints.

A schematic representation of the experimental setup used during the tests is presented in Fig. 2. The FSW process parameters used in the present investigation are provided in Table 2.

Tensile test samples were cut perpendicular to the welding direction as illustrated in Fig. 3a, with the sample dimensions prepared according to the ASTM E8. The final size of the transverse tensile test samples is shown in Fig. 3b, which includes the different parts of the joint: the (i) base metal (BM), (ii) heat-affected zone (HAZ), and (iii) SZ. Tensile tests were carried out at room temperature at a crosshead speed of 1 mm/min by using a screw-driven test machine. Vickers hardness measurement extending across the entire region with a spacing of 1 mm was conducted by using a Vickers indenter with a load of 10 N and a dwell time of 10 s in order to have the local properties of the different zones of the joint.

Table 1 Mechanical properties of the as-received base material Ti–6Al–4V

Property	Tensile strength (MPa)	Yield strength (MPa)	El. (%)	Hardness (VHN)
Value	994	910	17.2	344

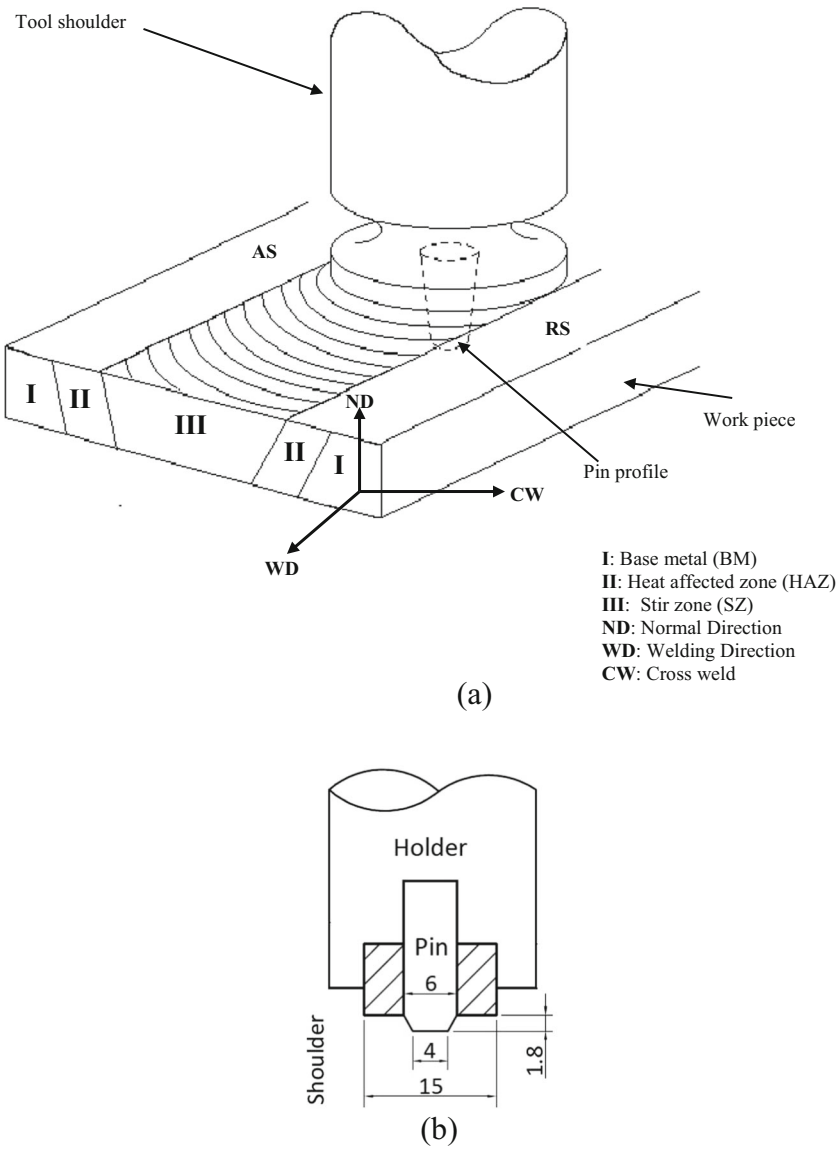

Fig. 1 **a** Schematic representation of FSW process showing the main characteristic zones and **b** shoulder and pin tool characteristics in millimeter

Specimens for optical microscopy (OM) and scanning electron microscopy (FEG-SEM) analyses were cut perpendicular to the welding direction and mechanically polished with 6, 3, and 1-μm diamond paste. The final polishing was accomplished by using colloidal silica of about 40 nm in diameter, followed by etching in Kroll's reagent (2 vol% HF and 4 vol% HNO_3 in water).

3 Results and discussion

3.1 Characteristics of the weld

The welded joints show a smooth surface appearance with no oxidation along the joint line. An illustrative example is shown in Fig. 4a, where a very little change in color can only be observed at the end of the weld line. This position corresponds to the tool removal after the end of the welding process, indicating that the argon protection system used in the present investigation is efficient in preventing surface oxidation of the welded joint. The optical micrographs of the cross sections perpendicular to the tool traverse direction for tool rotation rates of 1000 and 1500 rpm are presented in Fig. 4b, c, respectively. The different zones of the weld as well as the advancing and retreating sides are identified in these figures. The influence of the tool rotational speed on weld quality and the macrostructure of the joint are also evident in Fig. 4b, c. Thus, increasing the tool rotational speed from 1000 to 1500 rpm resulted in a defect-free macrostructure in the weld as shown in Fig. 4c. This finding may be related to the higher temperatures and therefore better material workability reached under high rotational speed welding conditions. Edwards and Ramulu [11] reported that rotational

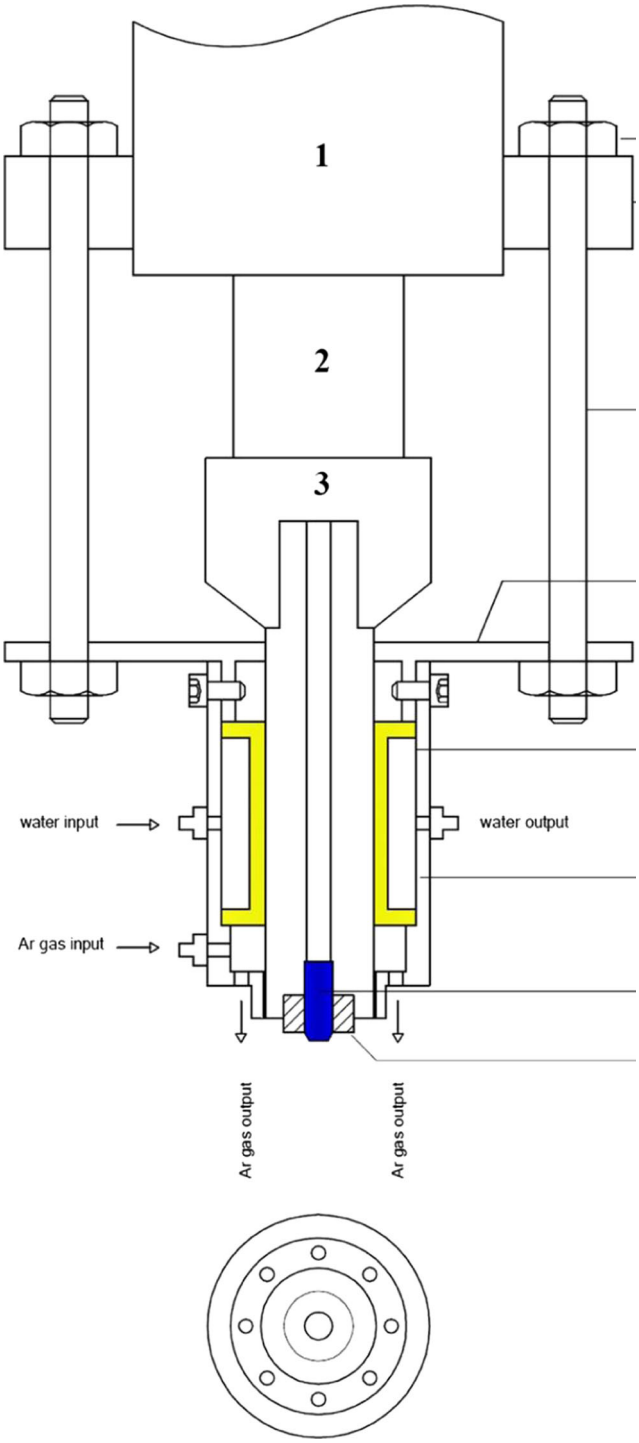

Fig. 2 Schematic of FWS system used in our experimental test. Fixed neck of the machine (*1*), removable neck machine (*2*), three systems and nut set (*3*)

speed has a large influence on peak temperatures reached during FSW of Ti–6Al–4V alloy. Raising the tool rotational speed from 1000 to 1500 rpm increases the weld temperature well above the alpha to beta transus temperature. The bcc beta phase being "softer" than the hcp alpha phase denotes a better workability. It is worth noting also that

Table 2 FSW welding parameter used on the samples

Weld number	Rotation [rpm]	Travel [mm/min]
1	1000	25
2	1000	50
3	1000	100
4	1250	25
5	1250	50
6	1250	100
7	1500	25
8	1500	50
9	1500	100

microscopic examination of the weld nugget for 1500 rpm conditions did not reveal the presence of kissing bonds or volumetric defects.

A small volumetric defect (lack of penetration) is observed at the root of the joint welded under cold welding conditions, i.e., tool rotational speed of 1000 rpm and a travel speed of 50 mm/min (Fig. 4a). Other commonly observed FSW defects [12, 13] such as kissing bonds, worm hole, and surface defects were also observed in some samples. For example, a surface defect is shown in Fig. 4a and a kissing bond defect, observed in the lower central region of the nugget, in Fig. 4b. It is interesting to note that, unlike friction stir-welded joints of aluminum alloys, there is no apparent thermomechanically affected zone (TMAZ) in the Ti–6Al–4V alloy weld, and the weld zone (WZ) consists only of the SZ and the HAZ. For clarification purposes, the boundaries between the different zones are separated by the white borderlines in Fig. 4b, c. The lighter zone is the BM, and the narrow gray zone (about 1 mm large) between the WZ and the BM is the HAZ. It is worth noting that the size of the HAZ in FSWed Ti–6Al–4V alloy is several orders of magnitude smaller than those observed in Al or Mg alloys as reported by Tongne et al. and Afrin et al., respectively [14, 15]. This may be related to the lower thermal conductivity of Ti (21.9) compared to that of Al (205) or Mg (156 W/m/K). Also, in Fig. 5a–c, the higher magnification microstructures of different zones (BM, HAZ, and SZ) associated with the rotational speed of 1000 rpm and travel speed of 50 mm/min are presented. Also, the microstructures in the same zones for the rotational speed of 1500 rpm and tool travel speed of 50 mm/min are shown in Fig. 5d–f.

The microstructure in the BM is characterized by elongated primary α and transformed β grains with an average grain size of 20 μm (see Fig. 5a, d). The evolution in the grain size and morphology from the BM to HAZ and then SZ is clearly visible in Figs. 4 and 5. For instance, the average grain size changes from 20 μm in the BM to about 15 μm at the start of the HAZ and then further reduces to 5 μm in the SZ. The influence of tool rotational speed on the evolution of the

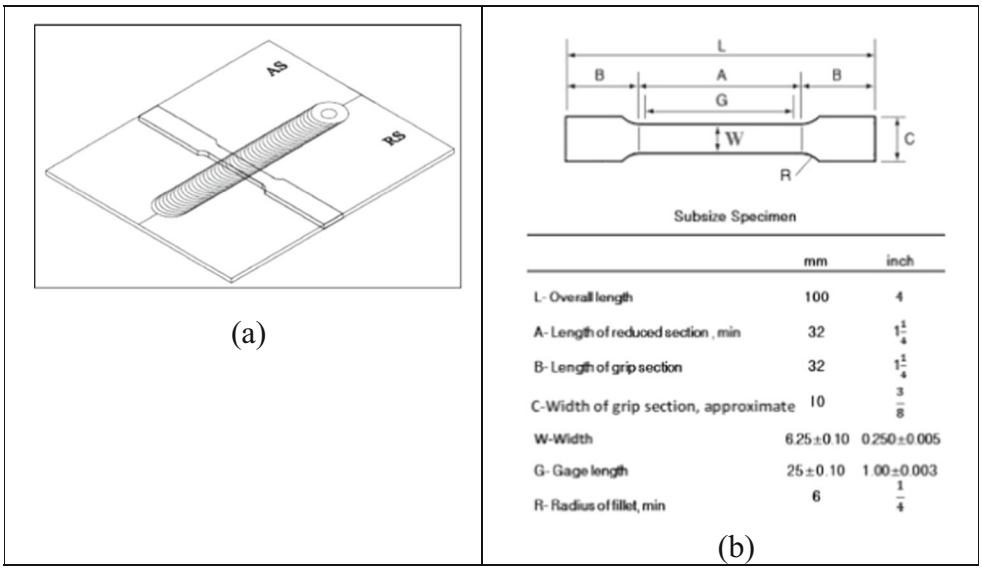

Fig. 3 Method of sampling for tensile test (**a**) and schematic of standard sample size based on the traversal tensile test (**b**)

microstructure from BM to HAZ is shown in Fig. 5b, e. A comparison between Fig. 5a, c shows that the grain size decreased noticeably in the weld joint (Fig. 5c) when compared to the base material (Fig. 5a).

An examination of the microstructures in the HAZ and the BM shows that they are very similar (Fig. 5b, e) for both tool rotational speeds. However, some lamellar α was observed in the HAZ indicating that the temperature in the HAZ went above the β-transus. While the residence time at high temperature has been very short for the investigated tool rotational speeds, it appears that it has been long enough to induce microstructural changes in the material.

For all the investigated process parameters, it can be observed that the microstructure of the SZ changes from one end to another across the weld joint as well as through the thickness of the sheet. The central SZ is characterized by a microstructure with small prior beta grains (5 μm) and fine lamellar alpha. By contrast, the top SZ is characterized by much finer and equiaxed grains with an average grain size of 1 μm (Fig. 5f). The presence of these grain morphologies for all the tested conditions suggests that their formation does not depend on the initial microstructure and is strictly controlled by the stirring process, i.e., deformation and the thermal cycle. Indeed, the absence of a lamellar microstructure in the upper region of the SZ indicates that the temperature in this zone did not exceed the β-transus, probably due to the cooling effect of the argon gas. The material was therefore mainly submitted to the stirring effect resulting in extensive grain refinement. This is in contrast to the microstructure in the center of the SZ, where lamellar structures are widely observed.

This evolution in the microstructure can be explained by the high temperatures and strains reached in the SZ during the FSW process that are above the critical levels for the initiation of recrystallization. Specifically, in the case of aluminum alloys, several mechanisms based on dynamic recrystallization (DRX) have been proposed to explain grain refinement in the SZ and have been summarized by several authors such as Mishra et al. and Sanders et al. [5, 7]. The mechanism of grain refinement in FSWed titanium alloys, however, is less discussed. Macrographic examination of the cross section of the weld joints obtained in the present investigation indicated that the SZ has a nominally bowl shape that flares out slightly near the surface where the tool shoulder contacts the work piece. The obtained results are in agreement with those reported by Sanders et al. and Ramirez et al. [5, 16] who observed an important grain refinement in the SZ during FSW and associated the formation of the fine grain structure to the occurrence of dynamic recrystallization (DRX).

The results also indicate that the microstructure of the nugget is not uniform in all regions and is particularly very dependent on the tool rotational speed (Figs. 8 and 9). According to the data, reported in the literature [16, 17], on FSW of α/β titanium alloys, the temperature in the SZ exceeds the β-transus, and thus, a fully lamellar microstructure is expected to be formed in this region. In the present work, for the highest tool rotational speed of 1500 rpm, the top surface layer of SZ has an equiaxed primary α with transformed β while the center of the SZ has a lamellar structure. By contrast, for lower rotational speeds of 1000 and 1250 rpm, only bimodal microstructures were observed in all regions of the SZ (Fig. 6).

The influence of tool rotational speed on the average grain size at the center of the SZ for a fixed tool travel speed of 50 mm/min is shown in Fig. 6a–c. It can be seen that as the tool rotational speed increases (i.e., transition from cold weld to hot weld), the average grain size in the center of the SZ progressively decreases. An average grain size of 10, 7, and 5 μm for 1000, 1250, and 1500 rpm, respectively, can be observed. The decrease in the average grain size with the increase in the rotational speed indicates that higher temperatures are achieved for tests employing higher stirring speeds,

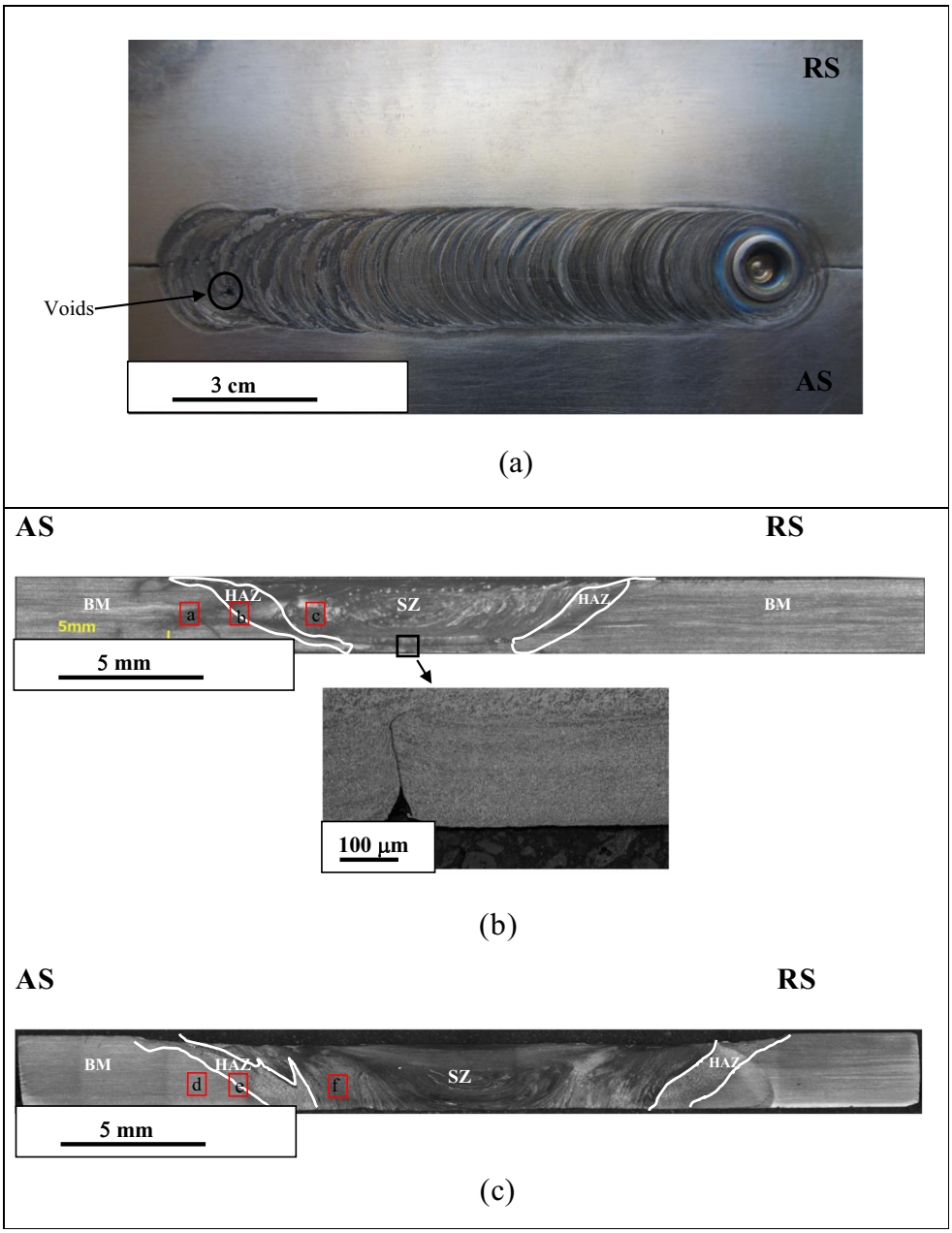

Fig. 4 Weld joint **a** macrostructure showing flow through both advancing and retreating sides **b** under 1000 rpm and **c** 1500 rpm of tool rotational speed and 50 mm/min of tool traverse speed in optical images. The *black lines* bordered the BM region HAZ and SZ

and therefore, finer grain sizes could be produced. For the highest rotational speed (i.e., 1500 rpm and 50 mm/min), as reported in Fig. 5f, a very fine microstructure of α grains is observed (Fig. 5f). However, when the rotational speed is decreased to 1250 rpm, the microstructure of the SZ changes to one composed of grain boundary α and lamellar α colonies formed within the prior β grains (Fig. 7). Moreover, a regular banded structure with an average grain size of 4 μm which consists of grain boundary and lamellar α is evident in the microstructure.

The obtained results indicate that the rotational speed is the most significant process variable. A high rotational speed (>1000 rpm) increases the applied strain rate and therefore influences the recrystallization process thereby influencing the quality of the FSWed Ti–6Al–4V joint [18]. Also, since higher tool rotational speed further increases the stirring temperature, a slower cooling rate is expected after welding. In contrast, lower rotational speed provides lower heat input which would yield to void defects due to lack of stirring. In addition, a decrease in the tool rotational speed reduces the total surface area of the SZ, thereby affecting the temperature distribution in the FSWed joint. The findings described above are in agreement with those reported by Pilchak et al. [17] for the friction stir processing (FSP) of Ti–Al–6V and Zhou et al. [18] for FSW of Ti–6Al–4V. A higher rotational speed causes excessive release of stirred material to the upper surface,

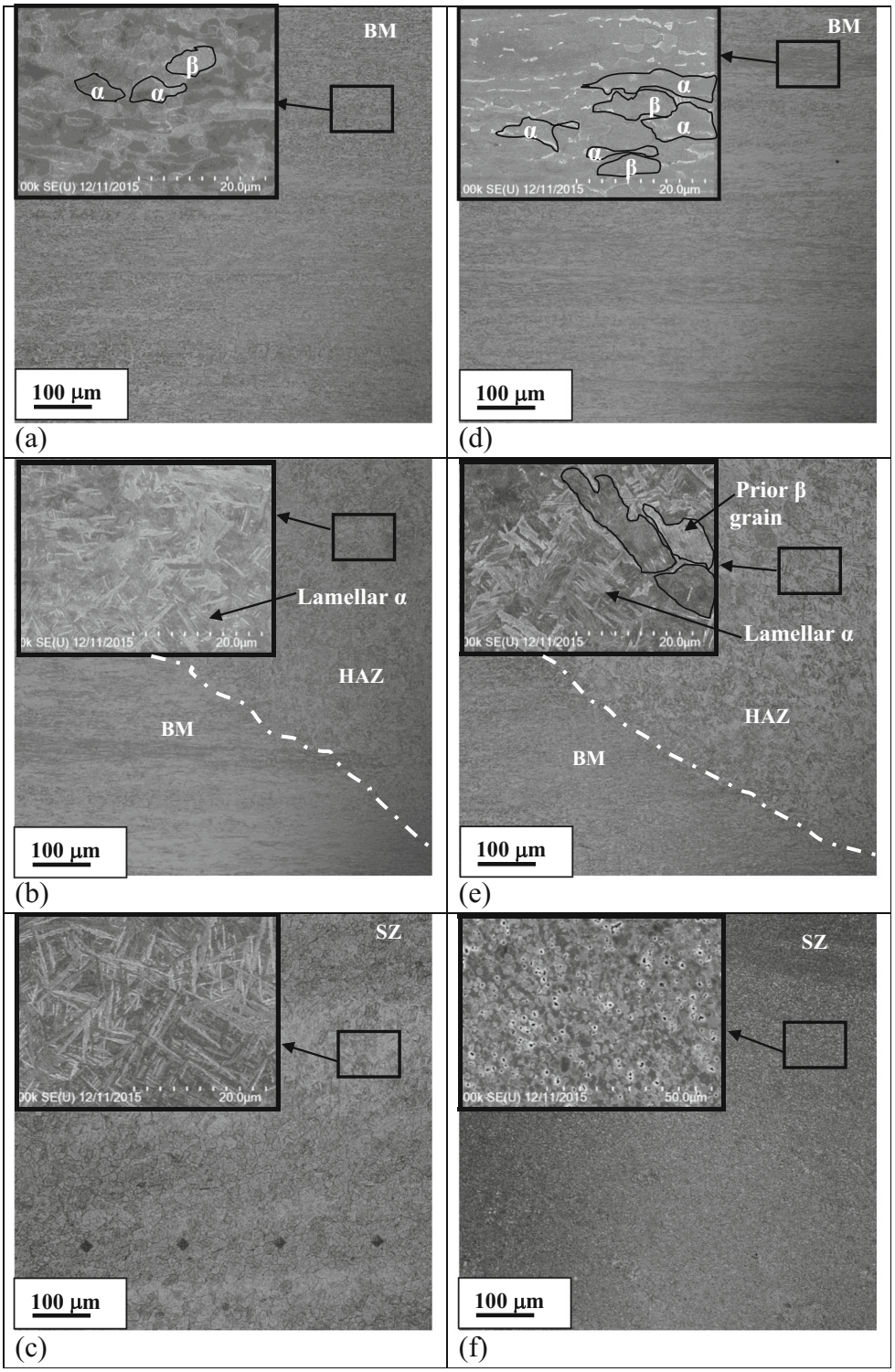

Fig. 5 Optical and SEM images showing the microstructure flow through advancing sides of the different weld region identified in Fig. 5 at 1000 rpm (**a**, **b**, and **c**) and 1500 rpm (**d**, **e**, and **f**)

resulting in the formation of voids in the stirred zone. Therefore, in order to achieve uniform microstructure in the SZ, the tool rotational speed should be the first process parameter to be optimized.

The influence of tool travel speed on grain size and phase characteristics is displayed in Fig. 7a–c. It can be seen that for the same tool rotational speed, when the travel speed is increased from 25 to 100 mm/min, a significant change in the β grain size is evident. Specifically, the average grain size decreases continuously as the travel speed is increased. Grain sizes of 15, 10, and 7 μm were achieved for 25, 50, and 100 mm/min, respectively (tool rotational speed of 1250 rpm). The significant grain refinement at the highest tool travel speed could be explained by the high strain rates applied

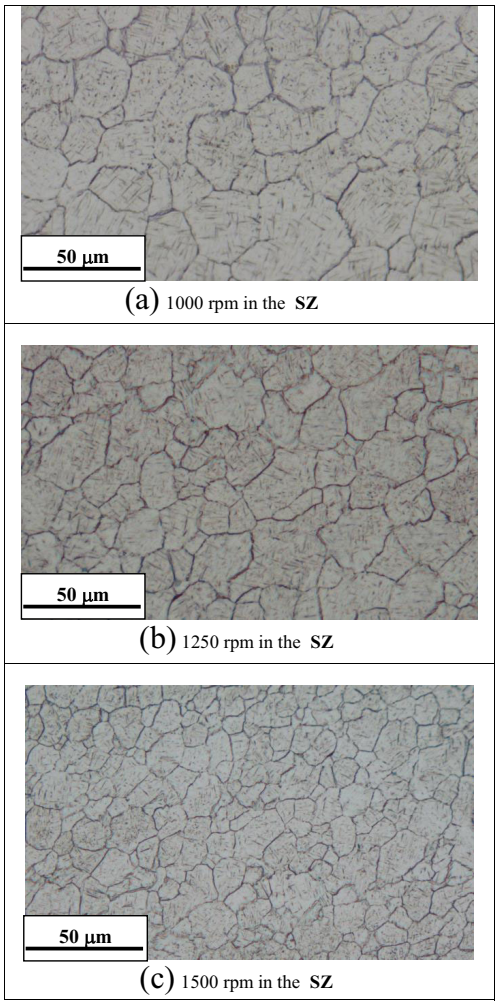

Fig. 6 Microstructure evolution in the stir zone with different rotational speed under a same tool travel speed of 50 mm/min optical images

to the material under these conditions. DRX is highly dependent on physical variables such as deformation, strain rate, and working temperature. Therefore, microstructure evolution is strongly associated with the nucleation rate and grain growth kinetics of DRX.

In hot working processes, DRX occurs if the true strain and strain rate reach a critical value. Since FSW is fundamentally a hot working process, it could be analyzed in terms of its process variables. Moreover, as in the FSW process strain, strain rate and temperature are significantly higher than, for example, in the forging process, it is expected that DRX should occur relatively easily during FSW. The combined effects of strain rate (ε) and deformation temperature (T) are often represented by a single parameter, the Zener–Hollomon parameter (Z), as defined by Zener et al. [37],

$$Z = \varepsilon \exp\left({}^{Q}/_{RT}\right) \tag{1}$$

where R is the gas constant and Q is the related activation energy for deformation.

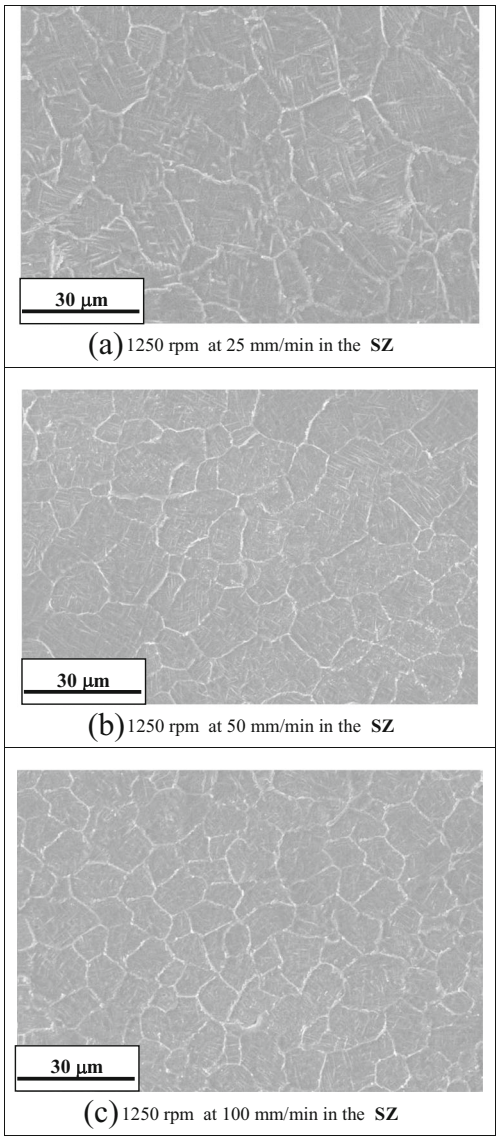

Fig. 7 SEM images of the SZs produced at different travel speeds: **a** 25 mm/min, **b** 50 mm/min, and **c** 100 mm/min. (Rotation speed = 1250 rpm)

A linear dependence between the Zener–Hollomon parameter and the applied stress has been reported by several authors [11, 19]. In general, the Zener–Hollomon parameter provides a basis for evaluating the evolution of the subgrain structure during hot deformation. As shown by Mc Queen et al. [20] in aluminum alloys, the following relations exist between the grain diameter d_{m} and the Z parameter,

$$d_m = [-0.60 + 0.08 \log Z]^{-1} \tag{2}$$

$$Z = \varepsilon \exp\left[\frac{18.77}{T_{\mathrm{p}}}\right] \tag{3}$$

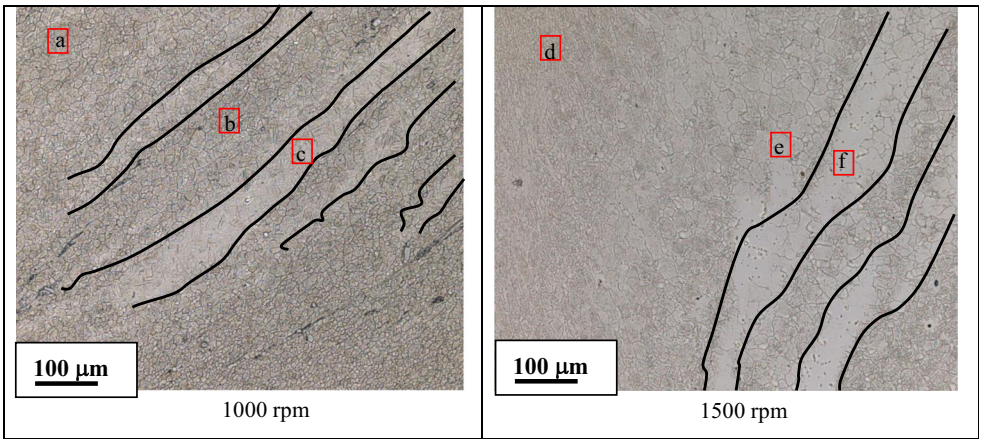

Fig. 8 Band structures in the SZ at different rotational speed and a 50-mm/min tool travel speed

In the above equations, T_p is the peak temperature of the thermal cycle (in Kelvin).

Edwards et al. [21] carried out experimental measurements to determine peak temperatures in the SZ of the FSWed titanium alloy as a function of various process parameters (Table 3).

The Zener–Hollomon parameter and the strain rate in the SZ were calculated from Eqs. (2) and (3) and are reported in Table 4. To this end, the peak temperatures reported in Table 3 and the grain sizes for different testing conditions reported in Sect. 0 were used.

The Zener–Hollomon parameter (Z) and the local strain rate in the SZ are between 25 and 120 s^{-1}, respectively. These values are higher than those reported by Frigaard et al. [38] for aluminum alloys (between 1 and 20 s^{-1}). However, in their case, the angular velocity of the tool was more than one order of magnitude higher than the one used in the present investigation. As angular velocity

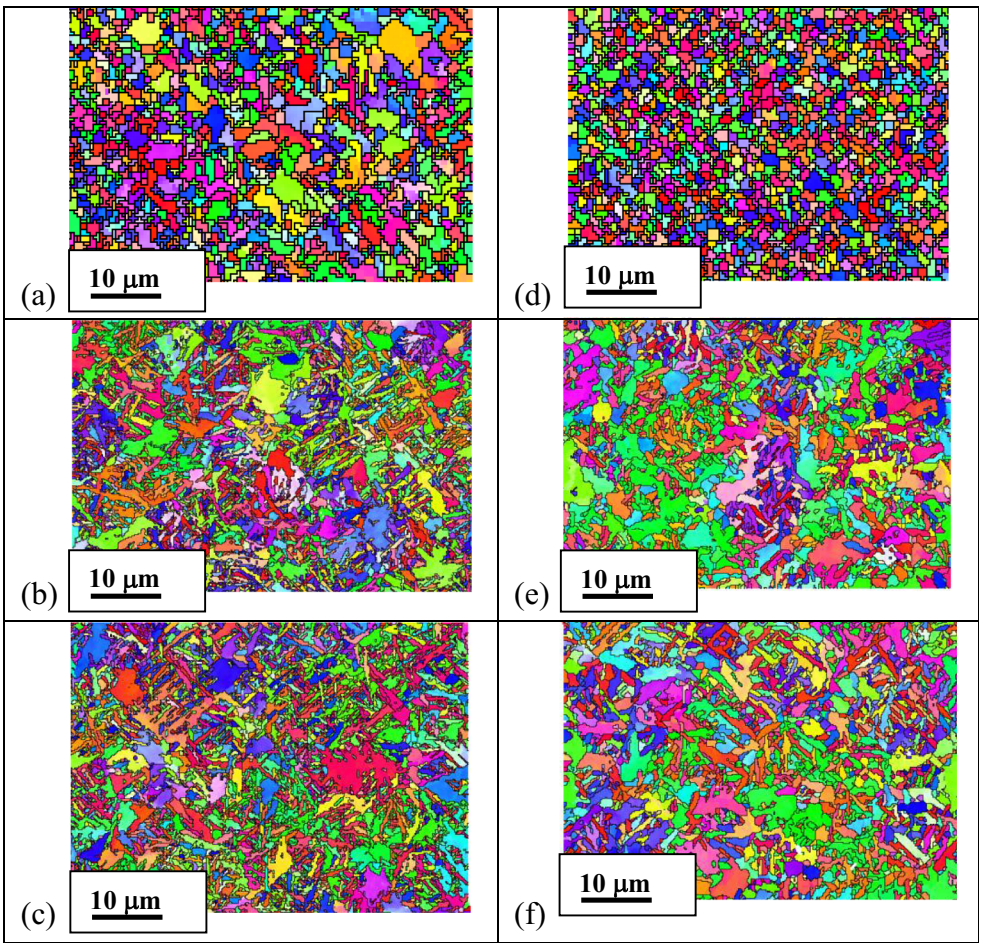

Fig. 9 EBSD images showing the grain morphologies in the SZ at region identified in Fig. 8 at 1000 rpm (**a**, **b**, and **c**) and 1500 rpm (**d**, **e**, and **f**) and 50-mm/min tool travel speed

Table 3 Peak temperature at different tool rotational speeds and 100 min/min of tool travel speed

Tool rotational speed (rpm)	Peak of temperature (°C) in the upper SZ	Peak of temperature (°C) in the lower SZ
150	1000	800
300	1000	1050
350	1150	1180

can directly affect the strain rate severity; therefore, the strain rate values obtained in this work could be considered reasonable. Based on the above calculations, the highest Z value is obtained for the highest tool travel (high strain rate) and tool rotational speeds (high temperature). The grain refinement is therefore pronounced at higher deformation conditions (higher Z), as shown in Fig. 7.

The grain refinement mechanism (i.e., DRX mechanism) in the SZ in titanium FSWed is widely discussed in the literature. However, as reported by Mironov et al. and Ding et al. [11, 22], the original equiaxed grains become thinner with a high aspect ratio, thus reflecting the strain increase in the SZ. The boundaries of the parent grains become wavy as the temperature increases and local boundary migration starts to occur.

Dislocation activities are the main controlling mechanisms of grain refinement [11, 23]. This is characterized by forming various dislocation configurations including dislocation cells and walls, geometrically necessary and incidental dislocation boundaries [23, 24]. The dislocation cells gradually transform into subgrains separated by boundaries of small misorientations (from dislocation cell walls). With increasing strain, misorientations of the subgrain boundaries increase, forming high-angle GBs so that refined grains are randomly oriented. The grain refinement mechanisms are probably similar for both high and low Z conditions [23]; however, it has been reported that during high Z deformation, dislocation rearrangements lead to a breakdown of the transformed microstructure during the FSW process. This provides a fine and equiaxed microstructure which is homogeneous along the weld joint [16] as observed in the present investigation (Figs. 5f and 6c).

Table 4 Zener–Hollomon parameter and strain rate estimation in the SZ

Tool rotational speed (rpm)	Zener–Hollomon parameter (s^{-1})	Strain rate (s^{-1})
1000	25	24.61
1250	75	73.83
1500	120	118.13

Table 5 Tensile properties of the base material and welded joints in transverse direction

No.	ω/ν	Yield strength (MPa)	Tensile strength (MPa)	Elongation (%)	Fracture zone
	BM	910	1150	17.2	
1	1000/100	838.5	944	8.8	SZ–HAZ boundary
2	1000/50	792	890	7	HAZ
3	1000/25	751	863	4	HAZ
4	1250/100	823	930	8.1	HAZ
5	1250/50	778	880.3	6.3	HAZ
6	1250/25	730	832	3.2	HAZ
7	1500/100	810	912	7.6	HAZ
8	1500/50	763	853.7	5.5	HAZ
9	1500/25	708.8	810.4	3	HAZ

3.2 Onion rings

The microstructure in the SZ is characterized by regular banded structures as shown in Fig. 8. The diagram in the right displays a different grain size compared to the neighboring zone microstructure. For instance, an average grain size of 4 μm was measured in the banded structure versus 7 μm outside this region. Different morphologies are also identified in the SZ at 1000 and 1500 rpm, respectively, outside the band and in the band structures as shown in Fig. 9. Thus, the presence of lamellar morphology in the band and the neighboring zone (Fig. 9b–f) and roughly equiaxed morphology (Fig. 9a, b) outside the bands is clearly demonstrated.

The origin of the banded structure is not well known in FSWed titanium alloys [25] and has not been discussed by many authors. Only, Wu et al. [25] reported the presence of such banded structures during FSP of Ti–6Al–4V alloy. However, as a first approach, this can be described as an onion ring-like structure. Onion rings are one of the most prominent features of friction stir welds and have been commonly

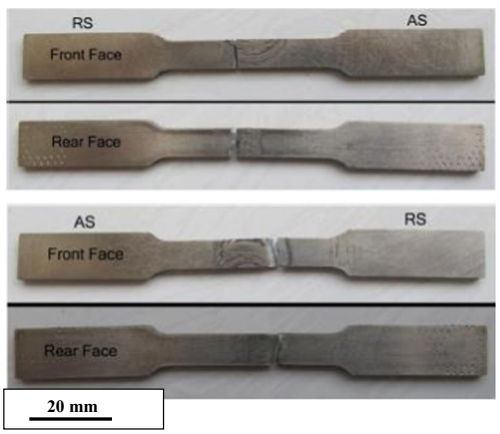

Fig. 10 Fracture localization of the FSW joints

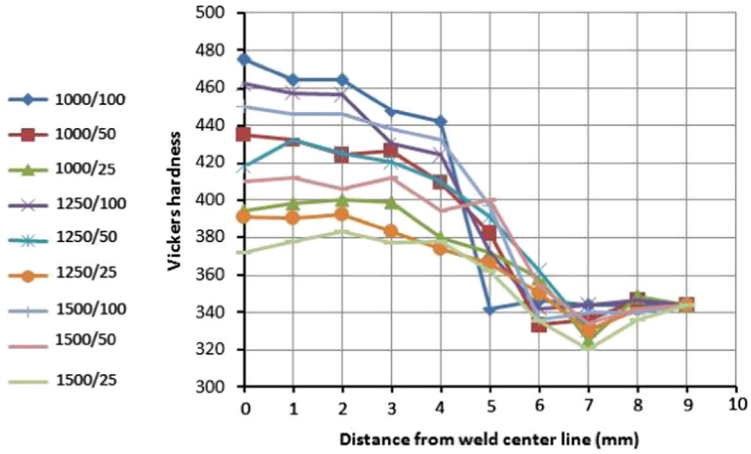

(a)

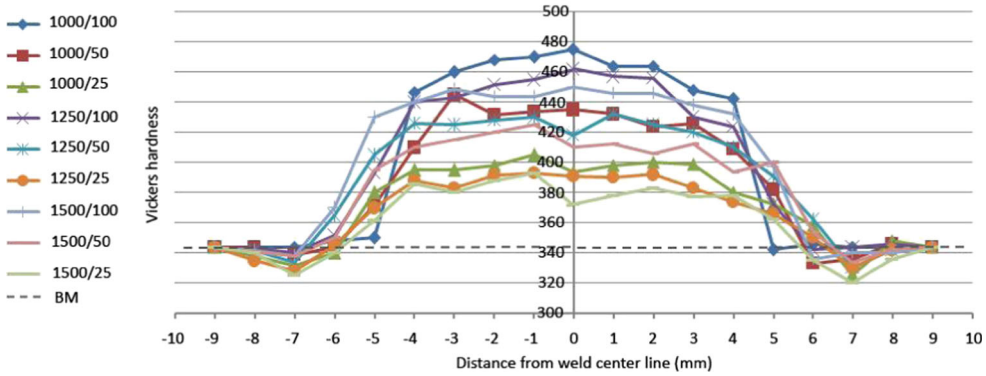

(b)

Fig. 11 Vickers hardness profiles **a** from the center of the SZ to the AS **b** across the whole joint of the welds produced at different rotational and travel speeds

reported in almost all aluminum alloys [14, 26]. While the influence of onion rings on mechanical properties of FSWed aluminum alloys is still debated, however many authors have related them to frictional heating due to the rotational and forward movement of the tool. This motion extrudes the metal and pushes it from the advancing side to the retreating side of the tool. The material is then compressed by each rotation of the tool [15, 26].

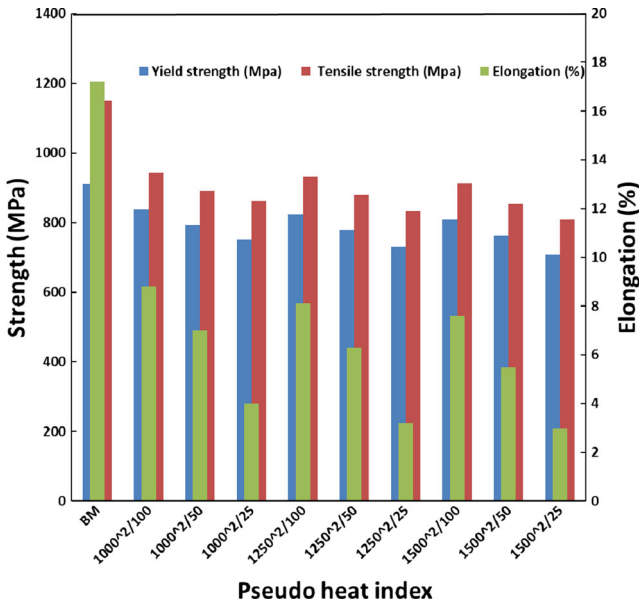

Fig. 12 Effect of pseudo heat index on transverse tensile properties

In the case of the titanium alloy studied in the present investigation, the difference in the microstructures present in the bands could also be related to differences in frictional heating, which could have resulted in increasing the temperature above the β-transus of the alloy in certain zones. As shown in Fig. 7a–c, both the prior β grain size and α colony size decrease with increasing rotational speed. This can further confirm the significant role of high heat generation on microstructure refinement.

3.3 Traverse tensile test

The tensile test results are summarized in Table 5. The main remarkable effect here is that for all the welding conditions, the samples failed in the HAZ. This zone has lower strength and elongation than the BM. Furthermore, as shown in the table, the mechanical properties decrease with increasing rotational speed. Note that all the welds fractured in the lowest

hardness region of the HAZ. For reference, the fractured surfaces of the samples after tensile tests are illustrated in Fig. 10.

Previous studies [27, 28] have shown that a friction stir weld with a heterogeneous hardness profile usually fails in the minimum hardness region and that the tensile properties of this area are representative of the transverse properties of the entire weld. In the present investigation, all the welds fractured in the HAZ during tensile tests. Therefore, the strength of the FSW joint will be considered as that of the HAZ in order to insure maximum reliability for the mechanical properties of the joint. The microstructure in the HAZ, for all welding conditions, is characterized by large grains compared with the SZ. As in high strength alloys, hardness is generally proportional to the yield strength [26, 29]; the lower strengths at higher rotational speed can be explained by the reduction of hardness in the HAZ, which is related to the coarser prior β grain size (Fig. 5e).

3.4 Hardness distribution across the joint

Microhardness measurements were carried out across the mid thickness of the joint to determine the effect of tool rotational speed and tool travel speed on hardness properties (Fig. 11).

In contrast to the tensile tests which provide the global properties of the joints, hardness measurements allow for the determination of local properties throughout the weld joint. As can be seen in Fig. 11a, b, the weld has a higher hardness compared to the BM. On the other hand, the lowest hardness can be observed in the HAZ. This hardness drop in the HAZ can be explained by the annealing effect caused by frictional heating in the HAZ. The heating effect, which is a function of the welding conditions, results in a change of the morphology in the HAZ. The mean hardness value of the SZ increases with increasing tool travel speed. When higher tool travel speeds are used, DRX in the SZ is not fully developed, thus increasing the hardness in the SZ [30].

The effect of rotational speed on hardness properties is also shown in Fig. 11a, b. It can be seen that, for all welding conditions used in this study, by increasing the tool rotational speed from 1000 to 1500 rpm at the same tool travel speed, the hardness of the SZ decreases. As mentioned in Sect. 0, the SZ experiences dynamic recrystallization during welding. It is also well known that recrystallization results in significant material softening [30, 31] which could explain the hardness decrease in the SZ.

3.5 Effect of pseudo heat index (ω^2/ν) on properties

The pseudo heat index defined by the ratio of the square of the rotational tool speed on travel speed is a well-known method to predict the heat generated during FSW as a function of process parameters. It was first introduced by Arbegast et al. [32] for FSWed aluminum alloys. For a given tool geometry and plunge depth, the maximum temperature highly depends on the rotational speed (ω, rpm) while the heating rate depends on the traverse speed (v, mm/min). The rotational speed term is squared due to its significant effect on the heat generated during the process [32, 33]. In the present study, the pseudo heat index parameter is used in order to determine the impact of the heat generated during FSW on mechanical properties of the Ti–6Al–4V FSWed joints.

The dependence of the strength and elongation of the joint on the pseudo heat index parameter is illustrated in Fig. 12. Specifically, it can be seen that an increase in the heat index parameter leads to a decrease in strength and elongation. The heat index parameters are $1000^2/100$, $1000^2/50$, and $1000^2/25$ for strengths of 838, 792, and 750 MPa, respectively. The corresponding elongations are also 8.8, 7, and then 4 %, respectively. This indicates that the pseudo heat index ratio can be used to describe the mechanical behavior of FSWed titanium joints. The decrease in strength and elongation with increasing the heat index parameter could also be related to microstructural changes in the titanium alloy associated with the process parameters.

As described above in Figs. 5 and 9, the changes in grain size and morphology during FSW of the Ti–6Al–4V sheets are closely related to process parameters such as tool rotational and tool travel speeds. On the other hand, microstructural analysis showed that under certain processing conditions, dynamic recrystallization could take place [34]. Therefore, the pseudo heat index parameter can be used as a simple tool to predict the evolution of the microstructure and mechanical properties of the FSWed Ti–6Al–4V. These findings are in agreement with those reported by Mironov et al. and Fratini et al. [35, 36] who found that an increase in the tool travel rate, or a decrease in the ratio of the tool rotational rate to tool travel speed, results in better mechanical properties of the weld joint.

4 Conclusions

Ti–6Al–4V plates with a thickness of 2 mm were successfully friction stir welded under different welding conditions. The mechanical properties of the joint were investigated by using tensile test and microhardness measurements for different welding heat index parameters.

The following conclusions can be drawn from this study:

1. The heterogeneous distributions of mechanical properties were directly related to the microstructure. It was shown that the SZ has the highest mechanical properties while the HAZ is the weakest region in the weld. The mechanical properties of the HAZ can be associated with the transverse tensile properties of the weld.
2. Mechanical properties of the FSW joint were correlated with the change in the microstructure, mainly in grain size

distribution. In addition, the $\beta \rightarrow \alpha + \beta$ phase transition in titanium alloys strongly influences microstructure evolution and therefore affects the mechanical properties of the joint.

3. The heat index can be used as a reliable parameter to describe the variations in strength and ductility of the joint.
4. The combined influence of temperature and strain, rather than temperature alone, is the key factor affecting the mechanical properties of the joint. Therefore, the tool rotational speed and the tool travel speed should be properly controlled to ensure good mechanical properties in FSWed Ti–6Al–4V alloys.

References

1. Lütjering G, Williams JC (2003) Titanium, vol 2. Springer, Berlin
2. Zwicker U (2007) Titanium and titanium alloys. Springer-Verlag, Berlin
3. Saresh N, Gopalakrishna Pillai M, Mathew J (2007) Investigations into the effects of electron beam welding on thick Ti–6Al–4V titanium alloy. J Mater Process Technol 192:83–88
4. Thomas WM, Nicholas ED (1997) Friction stir welding for the transportation industries. Mater Des 18(4):269–273
5. Sanders DG et al (2008) Characterization of superplastically formed friction stir weld in titanium 6Al-4 V: preliminary results. J Mater Eng Perform 17(2):187–192
6. Thomas WM, Threadgill PL, Nicholas ED (1999) Feasibility of friction stir welding steel. Science and Technology of Welding & Joining 4(6):365–372
7. Mishra RS, Mahoney MW eds (2007) Friction stir welding and processing. ASM international
8. Lee W-B et al (2005) Microstructural investigation of friction stir welded pure titanium. Mater Lett 59(26):3315–3318
9. Semiatin SL, Seetharaman V, Weiss I (1999) Flow behavior and globularization kinetics during hot working of Ti–6Al–4V with a colony alpha microstructure. Mater Sci Eng A 263(2):257–271
10. Edwards P, Ramulu M (2009) Effect of process conditions on superplastic forming behaviour in Ti–6Al–4V friction stir welds. Science and Technology of Welding & Joining 14(7):669–680
11. Ding R, Guo ZX, Wilson A (2002) Microstructural evolution of a Ti–6Al–4V alloy during thermomechanical processing. Mater Sci Eng A 327(2):233–245
12. Mehta KP, Badheka VJ (2016) Effects of tilt angle on the properties of dissimilar friction stir welding copper to aluminum. Mater Manuf Process 31(3):255–263
13. Sevvel P, Jaiganesh V (2015) Effect of tool shoulder diameter to plate thickness ratio on mechanical properties and nugget zone characteristics during FSW of dissimilar Mg alloys. Trans Indian Inst Metals 68(1):41–46
14. Afrin N et al (2008) Microstructure and tensile properties of friction stir welded AZ31B magnesium alloy. Mater Sci Eng A 472(1):179–186
15. Tongne A et al (2015) Banded structures in friction stir welded Al alloys. J Mater Process Technol 221:269–278
16. Ramirez AJ, Juhas MC (2003) Microstructural evolution in Ti-6Al-4V friction stir welds. Mater Sci For 426
17. Pilchak AL, Juhas MC, Williams JC (2007) Microstructural changes due to friction stir processing of investment-cast Ti-6Al-4V. Metall Mater Trans A 38(2):401–408
18. Zhou L et al (2009) The stir zone microstructure and its formation mechanism in Ti–6Al–4V friction stir welds. Scr Mater 61(6):596–599
19. Seshacharyulu T et al (2000) Hot working of commercial Ti–6Al–4V with an equiaxed α–β microstructure: materials modeling considerations. Mater Sci Eng A 284(1):184–194
20. McQueen HJ, Bourell DL (1987) Hot workability of metals and alloys. JOM 39(9):28–35
21. Edwards P, Ramulu M (2010) Peak temperatures during friction stir welding of Ti–6Al–4V. Science and Technology of Welding & Joining 15(6):468–472
22. Mironov S, Sato YS, Kokawa H (2009) Development of grain structure during friction stir welding of pure titanium. Acta Mater 57(15):4519–4528
23. Li YS et al (2009) Effect of the Zener–Hollomon parameter on the microstructures and mechanical properties of Cu subjected to plastic deformation. Acta Mater 57(3):761–772
24. Momeni A et al (2014) Microstructure evolution at the onset of discontinuous dynamic recrystallization: a physics-based model of subgrain critical size. J Alloys Compd 587:199–210
25. Wu LH et al (2014) Tool wear and its effect on microstructure and properties of friction stir processed Ti–6Al–4V. Mater Chem Phys 146(3):512–522
26. Krishnan KN (2002) On the formation of onion rings in friction stir welds. Mater Sci Eng A 327(2):246–251
27. Zhang Y et al (2008) Stir zone microstructure of commercial purity titanium friction stir welded using pcBN tool. Mater Sci Eng A 488(1):25–30
28. Ren SR, Ma ZY, Chen LQ (2007) Effect of welding parameters on tensile properties and fracture behavior of friction stir welded Al–Mg–Si alloy. Scr Mater 56(1):69–72
29. Edwards P, Ramulu M (2015) Fatigue performance of friction stir welded titanium structural joints. Int J Fatigue 70:171–177
30. Lütjering G (1998) Influence of processing on microstructure and mechanical properties of (α + β) titanium alloys. Mater Sci Eng A 243(1):32–45
31. Liu HJ et al (2003) Mechanical properties of friction stir welded joints of 1050–H24 aluminium alloy. Science and Technology of Welding & Joining 8(6):450–454
32. Arbegast WJ, Hartley PJ (2001) Method of using friction stir welding to repair weld defects and to help avoid weld defects in intersecting welds. U.S. Patent No. 6,230,957
33. Tang W, Guo X, McClure JC, Murr LE, Nunes A (1988) Heat input and temperature distribution in friction stir welding. J Mater Process Manuf Sci 7(2):163–172
34. Zhang Y et al (2008) Microstructural characteristics and mechanical properties of Ti–6Al–4V friction stir welds. Mater Sci Eng A 485(1):448–455
35. Fratini LIVAN et al (2010) A new fixture for FSW processes of titanium alloys. CIRP Annals-Manufacturing Technology 59(1): 271–274
36. Mironov S et al (2008) Crystallography of transformed β microstructure in friction stir welded Ti–6Al–4V alloy. Scr Mater 59(5): 511–514
37. Zener C, Hollomon JH (1944) Effect of strain rate upon plastic flow of steel. J Appl Phys 15(1):22–32
38. Frigaard Ø, Grong Ø, Midling OT (2001) A process model for friction stir welding of age hardening aluminum alloys. Metall Mater Trans A 32(5):1189–1200